

See discussions, stats, and author profiles for this publication at: <https://www.researchgate.net/publication/222090735>

Direct Measurement of the Three-Dimensional Product Velocity Distribution from Photoinitiated Bulb Reactions

ARTICLE *in* THE JOURNAL OF PHYSICAL CHEMISTRY · MARCH 1994

Impact Factor: 2.78 · DOI: 10.1021/j100064a018

CITATIONS

28

READS

30

5 AUTHORS, INCLUDING:



[Neil Shafer-Ray](#)

University of Oklahoma

64 PUBLICATIONS 983 CITATIONS

[SEE PROFILE](#)



[Richard P Tuckett](#)

University of Birmingham

162 PUBLICATIONS 2,086 CITATIONS

[SEE PROFILE](#)



[Richard Zare](#)

Stanford University

1,151 PUBLICATIONS 44,218 CITATIONS

[SEE PROFILE](#)

Direct Measurement of the Three-Dimensional Product Velocity Distribution from Photoinitiated Bulb Reactions

Neil E. Shafer, Hao Xu, Richard P. Tuckett,[†] Michael Springer, and Richard N. Zare*

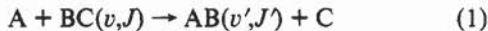
Department of Chemistry, Stanford University, Stanford, California 94305

Received: September 13, 1993; In Final Form: October 13, 1993[®]

We describe an apparatus designed to measure the velocity distribution of products of photoinitiated bulb reactions. A photolytic precursor AX and reactant BC are coexpanded into a vacuum chamber. A photolysis laser initiates the reaction sequence $AX + h\nu \rightarrow A + X$, $A + BC \rightarrow AB + C$. The C product is detected by sub-Doppler ($1+1+1$) resonance-enhanced multiphoton ionization (2D-REMPI) to yield its three-dimensional velocity distribution. If this technique were to be applied to the $AB(v',J)$ product, it would be possible to measure the alignment dependence of the state-to-state differential cross section. We present the experimentally determined velocity distribution of H atoms from the photolysis of HI and D atoms from the reaction $H + D_2 \rightarrow HD + D$, and we show that our measurements are consistent with previous studies.

1. Introduction

Consider a single reactive collision in which an atom A and a diatom BC in the internal vibrational-rotational state (v,J) collide and rearrange nuclei to produce the atom C and the diatom $AB(v',J')$:



For this collision process, the reactant approach trajectory, $r(t)$, can be written as

$$r(t) = vt + b \quad (2)$$

where the origin is chosen to be the center of mass of A, B, and C. In eq 2, v is the relative velocity of the reactants and b is a vector. Similarly, the product escape trajectory can be written as

$$r'(t) = v't + b' \quad (3)$$

To study the collision dynamics (as opposed to the potential energy surface of the A–B–C transition state) the reactants are prepared and the products are detected at times far removed from the collision time. In such studies the goal is to determine the probability of reaction as a function of $r(t)$ and $r'(t)$, or, equivalently, v , b , v' , and b' . Fortunately, each of the 12 components of these vectors, does not need to be specified to describe completely the dynamics of most reactions.

In the absence of an externally applied time-dependent force, the time origin of the reaction is arbitrary. In this case, the time origin may be taken so that b is orthogonal to v , or equivalently, so that $r(t=0) = b$, where b is the distance of closest approach of the reactants if they traveled in straight lines, i.e., the impact parameter. It is usually the case that b' is defined to be orthogonal to v' as well, but this definition does not reduce the number of free parameters. Instead, a new variable, Δt , must be introduced where Δt is the difference between the time origins used to describe the reactants and products, i.e., the interaction time.

In the absence of an anisotropy in space (such as an aligned reactant or an applied field), the orientation of the scattering process is arbitrary. If we reference the scattering process to the relative velocity of the reactants, v , only the magnitude of v must be specified, which reduces the number of remaining parameters

to nine. For the case of a scattering process that has cylindrical symmetry about v , the azimuthal angle of v' about v does not influence the dynamics. Hence, only eight independent variables must be specified. These may be taken to be the vector magnitudes v , b , v' , and b' , the scattering angle, $\theta_{vv'} = \cos^{-1}(b \cdot b')$, the dihedral angle between the plane containing v and v' and b , $\theta_{vv'-b}$, the dihedral angle between this plane and b' , $\theta_{vv'-b'}$, and the interaction time, Δt (Figure 1). Although no reactive scattering study to date has simultaneously specified each of these eight variables, the number of experimental constraints on these variables has steadily increased as experiments have gone from the measurement of scalars to vectors and to correlations between vectors.¹

In first-generation state-to-state reactive scattering studies, integral cross sections are determined for specified values of the $A + BC(v,J)$ collision energy. (For a review, see Bergmann and Rubahn.²) In these studies v and v' are specified by conservation of energy, but the parameters b , b' , $\theta_{vv'}$, $\theta_{vv'-b}$, $\theta_{vv'-b'}$, and Δt can take on any values that are consistent with the internal angular momentum quantum numbers, J and J' .

A second generation of state-to-state reactive scattering studies is dawning in which differential cross sections are being measured. Even though these highly sophisticated experiments are capable of specifying v , v' , and $\theta_{vv'}$, the parameters b , b' , $\theta_{vv'-b}$, $\theta_{vv'-b'}$, and Δt are only partially restricted. For this reason, a measurement of the state-to-state differential cross section does not give a complete description of the (asymptotic) reaction dynamics. A means must be found to determine b , b' , $\theta_{vv'-b}$, $\theta_{vv'-b'}$, and Δt .

The direct measurement of b and b' for a reactive scattering process would seem to be a daunting, if not an insurmountable, task. Conservation of angular momentum can be used, however, to reduce the number of undetermined variables. Specifically,

$$J + \mu b \times v = J' + \mu' b' \times v' \quad (4)$$

where J and J' are the internal angular momenta and μ and μ' are the reduced masses of the reactants and products. We regroup eq 4 to read

$$j = J' - J = \mu b \times v - \mu' b' \times v' \quad (5)$$

where j is the transfer of internal angular momentum in the reaction. The simultaneous measurement of v and v' and the three components of j could be used to parametrize b , b' , $\theta_{vv'-b}$ and $\theta_{vv'-b'}$ in terms of a single parameter.³ These considerations are purely classical. Of course, the uncertainty principle prevents us from either determining both b and v in the same measurement or specifying every component of j . The m_j dependence of a

* Permanent address: School of Chemistry, University of Birmingham, Edgbaston, Birmingham, B15 2TT, U.K.

[†] Abstract published in *Advance ACS Abstracts*, March 1, 1994.

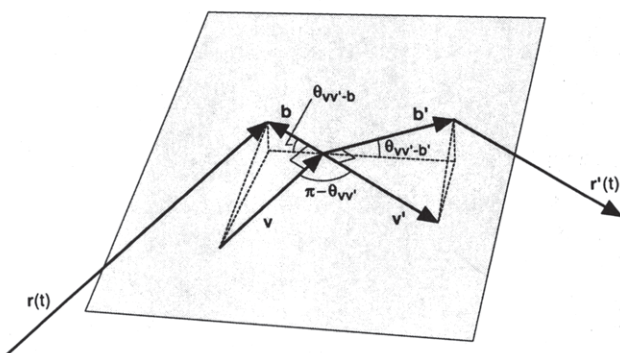


Figure 1. Illustration of the classical variables, v , v' , $\theta_{vv'}$, b , b' , $\theta_{vv'-b}$, and $\theta_{vv'-b'}$ needed to describe completely the asymptotic trajectories resulting from the collision of two unpolarized reactants A and BC to form the products AB and C.

differential cross section of a state-to-state reaction would, however, constrain b and b' to the extent possible by conservation of angular momentum.

A determination of the m_J -state populations and coherences is a difficult experiment that requires the measurement of the quadruple vector correlation between the relative velocity of the reactants, the relative velocity of the products, the alignment of the reactants, and the alignment of the products. A less difficult but important next step in the evolution of experimental reaction dynamics is the measurement of the triple vector correlation between the relative velocities of the reactants and products and the alignment of the product. Although such a measurement would not determine b , b' , $\theta_{vv'-b}$, and $\theta_{vv'-b'}$, it would place constraints on the geometry of the interaction and, by doing so, bring us one step closer to a complete picture of the dynamics of a bimolecular reaction.

In this paper we describe an apparatus designed to measure the alignment-dependent differential cross section of the $H + D_2(v, J) \rightarrow HD(v', J') + D$ reaction. Preliminary quantum mechanical calculations indicate that the additional constraints on the approach and escape trajectories imposed by the alignment of the $HD(v', J')$ product have marked dynamical consequences.⁴ Our strategy is to obtain the alignment-dependent differential cross section of the reaction from the alignment-dependent three-dimensional velocity distribution of the $HD(v', J')$ product of a photoinitiated bulb reaction. The relationship between this velocity distribution and the differential cross section is reviewed in section 2. In section 3 we describe the $(1 + 1 + 1)$ two-dimensional resonance-enhanced multiphoton ionization time-of-flight (2D-REMPI-TOF) technique. The apparatus is described in section 4. In section 5 we illustrate our experimental approach with measurements of the H-atom product velocity distribution from the photodissociation of HI, and the D-atom product velocity distribution from the photoinitiated reaction sequence $HI + h\nu \rightarrow H + I$, $H + D_2 \rightarrow HD + D$ at center-of-mass collision energies of 0.54 and 1.28 eV.

2. Differential Cross Sections from Product Velocity Distributions of Photoinitiated Bulb Reactions

The very small number of molecules that are produced in a given state and solid angle makes the measurement of a state-to-state differential cross section with a conventional crossed molecular beam apparatus a tour de force. To date, the product-state-resolved differential cross sections for the $D + H_2$ or $H + D_2$ reactions have been measured by only a few groups.⁵⁻¹⁰ Continetti⁷ and Schnieder and Welge⁹ were able to extract rovibrationally resolved product-state distributions from their experimental data. In the $D + H_2$ work of Continetti⁷ the HD product was probed by nonstate-specific electron impact ionization. In the $H + D_2$ work of Schnieder and Welge,⁹ the D-atom product was probed by Rydberg-atom TOF spectroscopy. Both

groups achieved state specificity by obtaining sufficient center-of-mass velocity resolution to resolve the quantized internal energies of the molecular products. If the alignment dependence of the differential cross section is to be determined, a direct state-specific probe of the $HD(v', J')$ product is required. To design an experiment that produces a detectable quantity of $HD(v', J')$ product, we have employed a photoinitiated bulb reaction.

In such a reaction, a precursor AX is photolyzed in the presence of a reactant BC to initiate the following sequence of events:



Information about the dynamics of the bimolecular reaction can be obtained by probing either the AB or C product. Recently, a number of workers have realized that the dependence of the laboratory-frame speed of the AB product, v_{AB} , on the center-of-mass scattering angle, $\theta_{vv'}$, can be used to obtain the differential cross section of the $A + BC$ reaction.¹¹⁻¹⁸ In the limit of a single collision energy for $A + BC$ and a translational temperature of 0 K for both AX and BC, the laboratory-frame velocity distribution of the AB product, $f(v_{AB})$, is related to the normalized differential cross section, $(1/\sigma)(d\sigma/d\Omega)$, by¹⁶

$$f(v_{AB}) = \left(\frac{1}{2v_{AB}u_{AB}} \right) \left(\frac{1}{\sigma} \frac{d\sigma}{d\Omega} \right) \left(1 + \beta P_2 \left[\frac{v_{AB}^2 + u^2 - u_{AB}^2}{2v_{AB}u} \right] P_2(\hat{v}_{AB} \cdot \hat{\epsilon}) \right) \quad v_{\min} < v_{AB} < v_{\max}$$

$$0 \quad v_{AB} < v_{\min} \text{ or } v_{AB} > v_{\max} \quad (8)$$

where

$$v_{\min} = |u - u_{AB}| \quad (9)$$

$$v_{\max} = |u + u_{AB}| \quad (10)$$

$P_2(x) = (3x^2 - 1)/2$ is the second-order Legendre polynomial, u is the speed of the center of mass, u_{AB} is the speed of the AB product in the center-of-mass frame, $\hat{\epsilon}$ is the polarization vector of the photolysis laser which is assumed to be linear, and $(1/\sigma)(d\sigma/d\Omega)$ is evaluated at

$$\cos \theta_{vv'} = \frac{v_{AB}^2 - u^2 - u_{AB}^2}{2uu_{AB}} \quad (11)$$

If the probe of the AB product is sensitive to the polarization of the molecule, the alignment-dependent state-to-state differential cross section can be determined.^{14,18}

A few groups have already taken advantage of the relation between the velocity distribution of the AB product and the differential cross section.^{11,13,15,17} In these studies, the projection of the AB velocity distribution onto the axis of a laser^{11,13,15} or a TOF tube¹⁷ was observed. Deconvolution¹⁷ or forward convolution^{11,13,15} schemes were used to gain information about the differential cross section, the alignment of the reaction products, or both. However, no example exists of a bulb experiment that directly measures the three-dimensional velocity distribution of the AB product.

We believe that there are two principal advantages to a measurement of the differential cross section in a bulb experiment. First, the entire differential cross section can be obtained from one TOF or Doppler profile without the need to rotate a detector in the laboratory frame. Second, higher pressures and hence higher product yields can be utilized. To take advantage of this increase in pressure, however, great care must be taken to minimize the effects of space charge, background, and secondary collisions. We have to create an apparatus that is sufficiently sensitive to measure the full three-dimensional velocity distribution of the

products of a photoinitiated bulb reaction by two-dimensional Doppler spectroscopy with an impulse-extraction TOF apparatus. In the following section we briefly describe the (1 + 1 + 1) 2D-REMPI TOF technique and the theory of velocity selection.

3. 2D-REMPI-TOF Detection of H and D

One of the most sensitive probes of the HD molecule that has been reported is (2 + 1) REMPI via the Q branch of the E,F¹ Σ_g^+ – X¹ Σ_g^+ transition coupled with TOF mass spectrometry.^{19–22} Although this probe has been used to measure the rovibrational distribution of the HD product of the photoinitiated reaction $\text{HX} + h\nu \rightarrow \text{H} + \text{X}$, $\text{H} + \text{D}_2 \rightarrow \text{HD}(v',J') + \text{D}$,^{23–25} this transition is not expected to be sensitive to alignment.²⁶ Therefore, it cannot be used to measure directly an alignment-dependent velocity distribution of the HD molecule. Furthermore, the high fluences required suggest that it may be difficult to measure the alignment-independent velocity distribution of the HD(v',J') product of a photoinitiated bulb experiment with this detection scheme. If a 1-cm⁻¹-bandwidth, 7-ns-pulsed laser is used to detect HD molecules by (2 + 1) REMPI via the E,F state, saturation of the E,F-X transition requires $\sim 10 \text{ J}\cdot\text{cm}^{-2}$ of 200–220-nm radiation. Under the relatively high-pressure conditions necessary to generate detectable quantities of reactive yield, this intense source of UV light creates sufficient nonresonant ions to overwhelm the detection system. Although these ions can be discriminated against by mass-gating the TOF apparatus,²⁷ it may be difficult to minimize the effect of the induced space charge. If instead HD is ionized via the one-photon B¹ Σ_u^+ – X¹ Σ_g^+ transition, calculated oscillator strengths²⁸ indicate that a fluence of only 10^{-2} – $10^{-4} \text{ J}\cdot\text{cm}^{-2}$ (for $v' = 0$ –3) of vacuum-UV radiation is required to saturate the transition. This 3–5 orders of magnitude reduction in the intensity of the probe laser greatly reduces the density of nonresonant ions. In addition, the use of a one-photon transition both provides sensitivity to alignment and allows us to take advantage of two-dimensional Doppler spectroscopy.²⁹ For these reasons, we are actively investigating the alignment-dependent 2D-REMPI detection of HD molecules. In what follows, we describe 2D-REMPI detection of H(D) atoms, which represents a first step to the above-stated goal.

If a sub-Doppler laser is used to excite the 1s → 2p transition in a hydrogen atom, the speed of the H atom along the axis of the laser beam is determined by the difference between the frequency of the resonant transition and the frequency of the laser. In our 2D-REMPI detection scheme, this transition is excited by a vacuum-UV laser beam that propagates along the x axis. Next, the H(2p) atom is excited to the 3d state with a visible laser that propagates along the y axis. Because this laser is also sub-Doppler, the speed of the H atom is determined along the x and y axes (two-dimensional Doppler selection). The H(3d) atom is then ionized with a third laser, and TOF spectroscopy is used to measure its velocity along the z axis. By this means, we determine each of the three Cartesian velocity components of the H atom. In our experiment, each probe laser is tuned to the center of its resonant transition. Thus, when an ensemble of atoms with a velocity distribution $f(\mathbf{v})$ is probed, we select $v_x = v_y = 0$ and measure $f(v_x = 0, v_y = 0, v_z)$. We call this function $f_{\text{exp}}(v)$. This ionization scheme is shown in Figure 2. A schematic of the experimental apparatus is shown in Figure 3.

Our 2D-REMPI-TOF scheme offers two advantages over TOF schemes^{30,31} that effect velocity resolution by constraining the field of view of a detector to include only those particles with a given velocity component perpendicular to the TOF axis. First, the angular resolution of our scheme is independent of the size of the ionization region. This feature allows for mass-selective detection of a large probe volume without compromising velocity resolution. Second, our technique is relatively insensitive to secondary collisions. Such collisions normally distort a velocity distribution by causing ions that would otherwise miss the detector

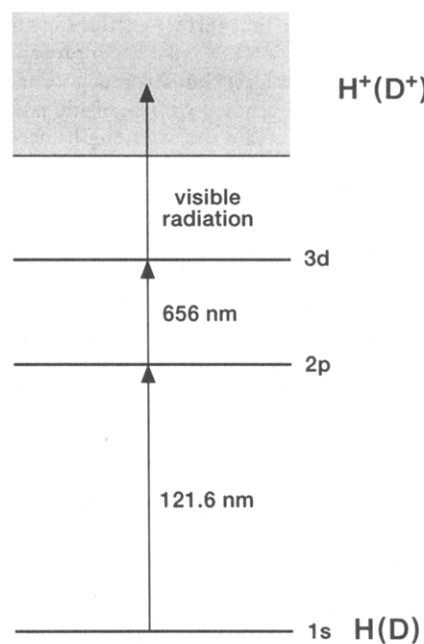


Figure 2. Two-dimensional resonance-enhanced multiphoton ionization (2D-REMPI) scheme for H and D atoms. A vacuum-UV laser selects the velocity along the x axis, and a visible laser selects the velocity along the y axis. Visible radiation is used to ionize the H(D) atom in the 3d state.

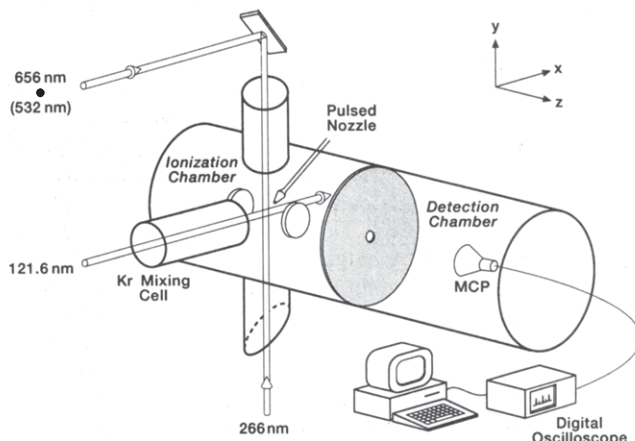


Figure 3. Schematic of the (1 + 1 + 1) 2D-REMPI-TOF apparatus. In the results presented in this paper, it is not necessary to use the 532-nm ionization laser for the detection of H⁺ (D⁺) ions.

to be steered toward it. Because all ions in our apparatus are produced with zero velocity perpendicular to the TOF axis, secondary collisions only lead to a reduction in signal intensity and not a distortion of the TOF profile.

4. Experimental Details

The experimental apparatus is divided into four sections: (1) the vacuum system, (2) the optical system, (3) the TOF apparatus, and (4) the data collection system. These parts of the apparatus are described in turn.

4.1. The Vacuum System. The vacuum system consists of an ionization chamber coupled with a differentially pumped TOF detection chamber. Both chambers are pumped with liquid-nitrogen-trapped diffusion pumps. Gas is allowed to enter the chamber through a 400-μs pulsed valve (General Valve 9-442-900, 0.8-mm orifice) that is synchronized to the 10-Hz laser system.

4.2. The Optical System. Four different laser beams can be used in our 2D-REMPI-TOF scheme: (1) a photolysis laser, (2) a v_x probe laser that excites the first transition of the probed

atom, (3) a v_y probe laser that further excites the atom, and (4) an ionization laser. The ionization laser copropagates with the v_y laser and the photolysis laser counterpropagates with v_y . This geometry allows for independent control of the polarization of the photolysis laser. To create the wavelengths needed, three 7 ns, Nd:YAG lasers can be used: (1) the fourth (266 nm) harmonic of a Nd:YAG laser (Spectra Physics, DCR-3) serves as the photodissociation pump beam, (2) a seeded Nd:YAG laser (Spectra Physics, GCR-4) pumps three dye lasers to create the probe beams necessary to excite the $1s \rightarrow 2p \rightarrow 3d$ transitions of the H (D) atom, and (3) the second (532 nm) harmonic of a Nd:YAG laser (Spectra Physics, DCR-1) may be used to ionize the doubly excited H atom. For the experiments presented in this paper, however, sufficient sensitivity is obtained when ions from the $3d \rightarrow H^+(D^+)$ transition induced by the v_y probe laser are observed. Hence, the third Nd:YAG laser is not used. The timing between these lasers is synchronized with digital delay generators (Stanford Research Systems, DG535) interfaced to an IBM-compatible computer.

The $1s \rightarrow 2p$ transition of the H (D) atom requires 121.6-nm vacuum-UV radiation. We create this wavelength by resonant four-wave mixing in Kr^{32,33} via the $4p^6 ^1S \rightarrow 5p' [0^1/2]$ transition at 202.315 nm (ω_1). One millijoule of this UV radiation is created by frequency tripling the output of a Spectra Physics PDL dye laser pumped with 84% (480 mJ) of the second harmonic of the GCR-4 Nd:YAG laser. This radiation is then combined with the output of a second dye laser (Lambda Physik, LPD 3000) pumped with 12% (70 mJ) of the second harmonic of the GCR-4 Nd:YAG laser; the dye laser wavelength is 602.5 nm (ω_2). The copropagating beams are focused together in a Kr cell to create ($2\omega_1 - \omega_2$) vacuum-UV radiation. The Kr cell is isolated from the vacuum chamber by either a 1 mm thick LiF window or a 150 mm focal length MgF₂ lens. This optic is heated to prevent pump oil from collecting on it. The Kr cell contains a liquid-nitrogen-cooled finger which maintains the Kr pressure at the near-optimal value of ~1 Torr. The liquid nitrogen trap also eliminates contamination caused by outgassing of the stainless-steel cell, thereby increasing the stability of the source from ~15 minutes to greater than 5 h. The vacuum-UV radiation can be focused by a cylindrical MgF₂ lens to the center of the ionization chamber. The vacuum-UV pulse energy in the interaction region is measured by flowing acetone vapor between two copper plates placed inside the ionization chamber. From the amount of charge induced on the plates at a given pressure, and with knowledge of the ionization cross section, we estimate that 700 nJ passes through the probe region when the LiF window is used, and 50 nJ when the window is replaced by the two MgF₂ lenses. The 656-nm radiation needed to excite the $2p \rightarrow 3d$ transition is produced by the third dye laser (Lambda Physik, LPD 3000) pumped by 1.4% (8 mJ) of the output of the second harmonic of the GCR-4 Nd:YAG laser. Etalons can be placed in any of the three dye lasers, which allows us to set the bandwidth of the vacuum-UV probe laser beam to either 2.4, 0.5, or 0.2 cm⁻¹, and the visible probe laser beam to either 0.2 or 0.05 cm⁻¹.

4.3. The TOF Apparatus. The velocity distribution of H(D) atoms is measured by time of flight using a technique we call impulse extraction. Here, a pulsed field is applied immediately after the ions are created, and the field is turned off before the ions exit the excitation regions (Figure 4). Details of the performance of this type of TOF analyzer are given in Appendix, section A.1. Great care is taken to ensure a uniform field in the extraction region. Four stacks of five resistively divided U-shaped plates are placed between the repeller and extractor plates (Figure 5). The total resistance between the repeller and the extractor (200 Ω) is matched to that of the high-voltage pulser (Avtech AVX-MRA2-AVR-A-1) which is used to accelerate ions out of the extraction region. This design allows us to cross the lasers in the center of the field-free region and bring the metal nozzle

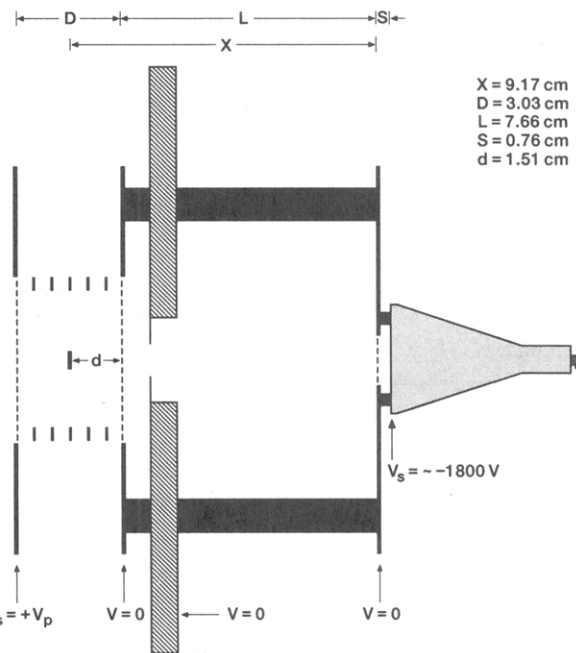


Figure 4. Schematic of the impulse-extraction TOF apparatus. V_p is the voltage applied to the repeller plate. It is turned off before an ion reaches the extractor plate (see Appendix A.1).

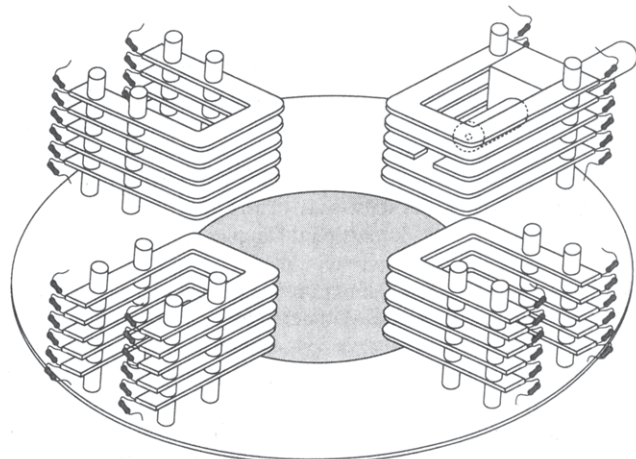


Figure 5. Design of the extraction region of the TOF apparatus.

to within 12 mm of the center of extraction region without distorting the field. In this manner, we can obtain a H-atom velocity resolution of 1.7 km·s⁻¹.

4.4. Data Collection. Ions are detected at the end of the TOF tube by an impedance-matched multichannel plate (Galileo Electro Optics, TOF-2003) interfaced to a 2-GHz sampling rate, 500-MHz digital oscilloscope (Tektronix TD-620). The scope is interfaced to a 50-MHz IBM-PC compatible computer (Los Altos Computers). Because data can be transferred at the repetition rate of the pulsed lasers (10 Hz), real-time data processing can be achieved, which allows us to use the oscilloscope and computer system as either a charge integrator or a multichannel scalar.

5. Results and Discussion

5.1. The Photodissociation of HI at 266 nm. In this study HI (Matheson, 98% purity) is purified by a freeze-pump-thaw procedure, diluted in a 1:3 ratio with He (Linde 99.999%), and expanded through the pulsed nozzle. The HI is photolyzed with linearly polarized, 266-nm radiation (3.3×10^{-2} J·cm⁻²). Lasers with fluences of 10^{-6} and 10^{-3} J·cm⁻² are used to excite the 121.6-nm $1s \rightarrow 2p$ and 656-nm $2p \rightarrow 3d$ transitions, respectively. Visible

radiation ionizes the H(3d) atom. The bandwidths of the 121.6- and 656-nm lasers are 2.0 and 0.2 cm⁻¹, respectively. The H⁺ signal increases with nozzle backing pressure from 50 to 200 Torr, and then levels off from 200 to 400 Torr. No significant difference in the H⁺ TOF profile is observed over the entire pressure range, which indicates an insensitivity of the apparatus to secondary collisions.

Interference and anisotropy effects were considered theoretically by Mukamel and Jortner^{34,35} for the general case of the photodissociation of a diatomic molecule. The photodissociation dynamics of HI have been studied extensively.³⁶⁻⁴² When the HI bond is dissociated by 266-nm radiation, the H atom acquires one of two velocities: $v_0 = 17.47 \text{ km}\cdot\text{s}^{-1}$, corresponding to the production of ground-state I(²P_{3/2}), or, $v_1 = 11.23 \text{ km}\cdot\text{s}^{-1}$, corresponding to the production of I*(²P_{1/2}). The channel leading to the faster H atom has an anisotropy parameter, $\beta_0 = -1$, whereas the channel leading to the slower H atom has an anisotropy parameter $\beta_1 = +2$. The only undetermined parameter needed to describe the velocity distribution of the H-atom photoproduct, $f(v)$, is the fractional yield of I*(²P_{1/2}), α . The velocity distribution of the H-atom product of the photodissociation of a 0 K HI gas by linearly polarized light may be written in terms of this parameter:

$$f(v) = (1-\alpha) \left(\frac{\delta(v-v_0)}{4\pi v_0^2} (1 - P_2(\hat{\epsilon} \cdot \hat{v})) \right) + \alpha \left(\frac{\delta(v-v_1)}{4\pi v_1^2} (1 + 2P_2(\hat{\epsilon} \cdot \hat{v})) \right) \quad (12)$$

Given this distribution, we expect to observe four peaks in the axial velocity distribution, corresponding to fast and slow H atoms moving toward and away from the detector. To make a detailed comparison of this distribution to our experimental data, we first convolute $f(v)$ with the spread in v_x and v_y (determined by the bandwidth of the two probe lasers) to find the distribution of the H⁺ velocities, $f_{xy}(v_z)$. We then convolute $f_{xy}(v_z)$ with our instrument function (see Appendix, section A.2) to find the expected TOF profile, $g_{\text{calc}}(t)$. A Jacobian transformation of $g_{\text{calc}}(t)$ yields the calculated velocity distribution, $f_{\text{calc}}(v)$. Full details of this analysis are given in Appendix, section A.2. Experimental and calculated TOF profiles are shown in Figure 6, a and b, for the cases that the photolysis laser polarization is perpendicular to and parallel to the TOF axis, respectively. The corresponding velocity distributions are shown in Figure 7, a and b. Note that, whereas the velocity distributions are approximately symmetric about $v = 0$, the TOF profiles are asymmetric. The long TOF peak has less height and more width than the short TOF peak. The form of this profile is a consequence of the Jacobian transformation.

The fits are good, but not ideal. The mismatch is a result of the fine structure splitting between the 2²P_{3/2} and 2²P_{1/2} levels of the H atom. This 0.356 cm⁻¹ splitting creates a velocity spread of $\Delta v_x = 1.3 \text{ km}\cdot\text{s}^{-1}$ and $\Delta v_y = 7.0 \text{ km}\cdot\text{s}^{-1}$. For an ideal system, the effect of this splitting is easily modeled.¹² Unfortunately, with our TOF apparatus we are unable to detect the entire population of H atoms with this large a spread in radial velocities. This inability causes a bias in our signal intensity that limits the accuracy of the simulation of the data and, consequently, our determination of the photodissociation branching ratio. If we compare the TOF intensity of the fast and slow H atoms that originally move toward (i.e., $v > 0$) the detector, we find $\alpha = 0.35 \pm 0.01$. On the other hand, when the fast and slow backward-scattered (i.e., $v < 0$) H atoms strike our detector, we find $\alpha = 0.41 \pm 0.04$. We conclude that $35 \pm 6\%$ of the I product is produced in the I*(²P_{1/2}) state. This percentage agrees with the value determined by Clear, Riley, and Wilson³⁶ ($36 \pm 5\%$), and by Schmiedl et al.³⁷ ($40 \pm 5\%$).

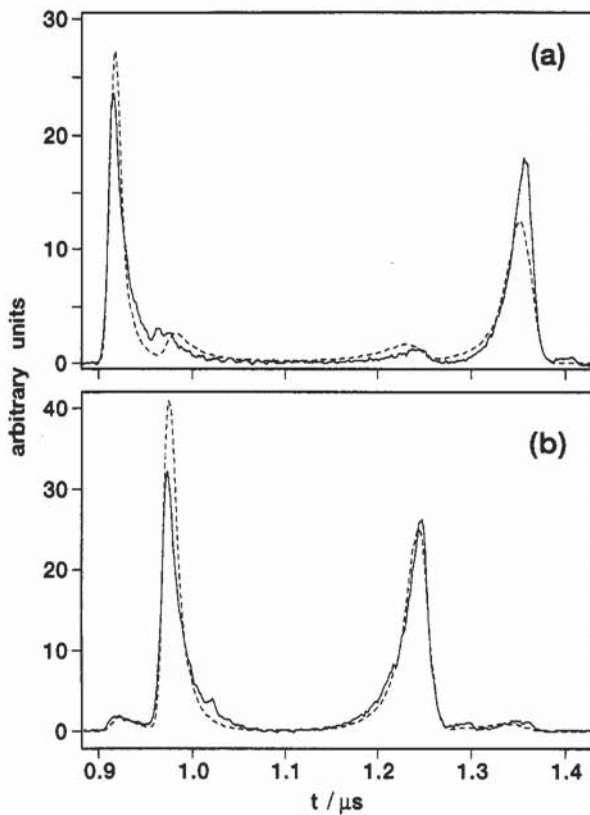


Figure 6. Calculated (dashed line) and experimental (solid line) TOF profile of H atoms from the photolysis of HI at 266 nm with the laser polarization (a) perpendicular to and (b) parallel to the TOF axis.

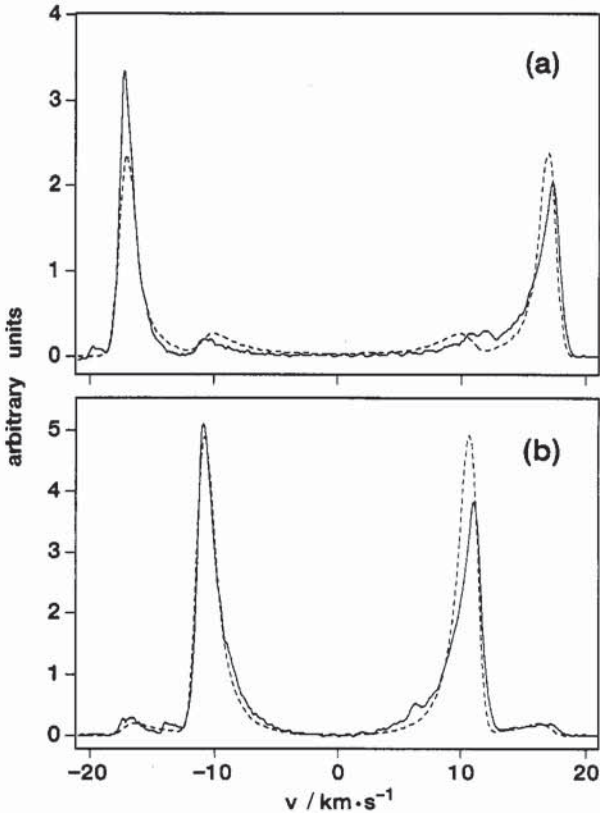


Figure 7. Calculated (dashed line) and experimental (solid line) velocity distribution, $f_{\text{calc}}(v)$, of H atoms from the photolysis of HI at 266 nm with the laser polarization (a) perpendicular to and (b) parallel to the TOF axis.

5.2. The Photoinitiated Reaction: HI + $h\nu$ (266 nm) → H + I, H + D₂ → HD + D. For this study, a 200 Torr, 1:10 mixture of HI (Matheson 98%) and D₂ (Linde 99.8%) is pulsed into the

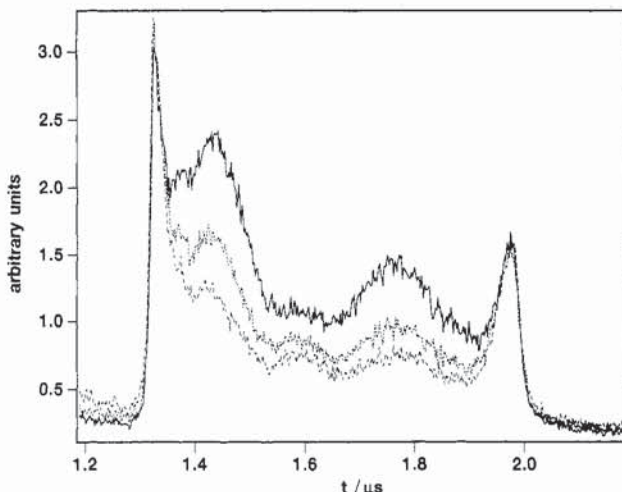


Figure 8. TOF spectra of the D-atom product from the $H + D_2 \rightarrow HD + D$ reaction at collision energies of 0.54 and 1.28 eV, initiated by the photolysis of HI at 266 nm. Also present are D atoms from the prompt photolysis of DI impurity in the HI. The time delay between the photolysis and probe lasers is 100 ns (solid line), 60 ns (dotted line), or 20 ns (dashed line). The D-atom signal from the bimolecular reaction grows in as the time delay increases. Also note the asymmetry in the photolytically produced D-atom peaks at 1.3 and 2.0 μs . This asymmetry arises from the Jacobian transformation of velocity to time (eq A.15).

extraction region. The HI is photolyzed by linearly polarized, 266-nm laser radiation ($2.4 \times 10^{-2} \text{ J} \cdot \text{cm}^{-2}$). The direction of the polarization is perpendicular to the TOF axis. After a computer-controlled time delay that alternates every 100 shots between 20, 60, and 100 ns, the D-atom product is ionized and detected via 2D-REMPI-TOF. Probe-laser wavelengths, fluences, and bandwidths are similar to those used in the study of the photolysis of HI. The dependence of the TOF profile on the delay between the photolysis and probe lasers is shown in Figure 8. The peaks in the TOF profile at 1.3 and 2.0 μs are caused by the photolysis of DI contaminant in our gas mixture. The ratio of the magnitude of this background to the reactive signal is consistent with that expected if the D atom arises from its naturally occurring isotopic abundance (0.015%).

The D-atom TOF distribution from the bimolecular reaction must be consistent with conservation of energy. Because the $H + D_2 \rightarrow HD + D$ reaction is thermoneutral, no D-atom product may have more kinetic energy than that of the H-atom reactants. Because the bond strengths of HI and DI are very similar, the background D atoms have the same amount of kinetic energy as the fast H-atom reactant. The photoproduct D-atom signal can therefore provide an immediate test of conservation of energy. All the reactive D-atom signal must have a TOF that lies between the TOFs of the long and short background peaks, which is indeed observed (Figure 8).

Because the photodissociation background signal does not increase with the pump-probe time delay, the velocity distribution of the D-atom product of the bimolecular reaction can be found by subtracting the signal obtained at 20 ns from that obtained at 100 ns (Figure 9). The corresponding velocity distribution of the D-atom product is shown in Figure 10. This velocity distribution is the sum of many distribution functions of the form of eq 8, each corresponding to a single $HD(v',J')$ state. Further averaging is brought about by the two possible collision energies (0.54 and 1.28 eV), corresponding to the two possible states of the I-atom photoproduct. Although the highly averaged D-atom velocity distribution is somewhat insensitive to the dynamics of the $H + D_2$ reaction, it serves as an excellent test of the feasibility of the more interesting state-to-state experiment in which the $HD(v',J')$ product is probed. To calculate the product D-atom velocity distribution, we consider both the kinematics and dynamics of this reaction.

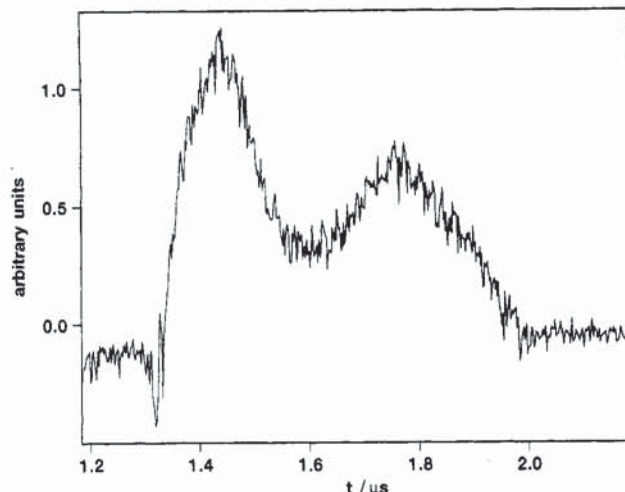


Figure 9. TOF spectrum of the D-atom product of the $H + D_2 \rightarrow HD + D$ reaction. This spectrum is obtained by subtraction of the signal for a 20-ns time delay (dashed line of Figure 8) from that for a 100-ns time delay (solid line of Figure 8).

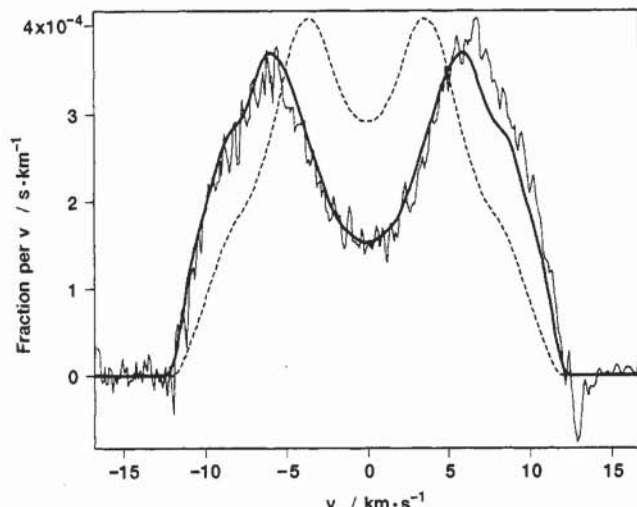


Figure 10. Velocity spectrum of the D-atom product of the $H + D_2 \rightarrow HD + D$ reaction. Experimental data (solid, noisy line) is compared to calculation when a hard-sphere cross section is assumed for every $HD(v',J')$ reaction channel (dashed line), and when the J' -dependent cross sections from Zhang and Miller⁴⁴ for the reaction $D + H_2(v=0,J=0) \rightarrow HD(v'=0,J') + H$ at a collision energy of 1.25 eV are assumed (solid, smooth line).

Kinematics determine the speed of the center of mass, u , and the speed of the D atom in the center-of-mass frame, u_D . The speed of the center of mass is given by

$$u = \left(\frac{m_H}{m_{D_2} + m_H} \right) v \quad (13a)$$

where v is the speed of the H atom. For the fast channel, $u = 3.50 \text{ km} \cdot \text{s}^{-1}$, for the slow channel, $u = 2.25 \text{ km} \cdot \text{s}^{-1}$, and the fraction of fast H atoms is 0.65, as determined in section 5.1. The speed of the D atom in the center-of-mass frame, u_D , is given by

$$u_D = \left(\frac{m_D}{m_{D_2} + m_H} \right) \left[\frac{\mu v^2 - 2\Delta E}{\mu'} \right]^{1/2} \quad (13b)$$

Here u_D depends on the difference between the internal energy of the products and reactants, ΔE . For this reason, u_D varies with the internal state of the product. For example, when $D_2(v=0,J=0)$ reacts with the fast H atoms to yield $HD(v'=2,J=5)$, $u_D = 4.35 \text{ km} \cdot \text{s}^{-1}$, but if $HD(v'=0,J=0)$ is formed, $u_D = 8.42 \text{ km} \cdot \text{s}^{-1}$.

Dynamics determine the relative yields of each $\text{HD}(v', J')$ product, as well as the v', J' -dependent differential cross sections for the reaction. The relative yields of $\text{HD}(v', J')$ can be taken as the product of the cross sections calculated by Blais and Truhlar⁴³ and the velocity of the H-atom reactant. To simplify our analysis, we only consider the reaction with $\text{D}_2(v=0, J=0)$. In addition, only the 35 most significant reaction channels are considered. They are $\text{H}(\text{fast}) + \text{D}_2 \rightarrow \text{HD}(v'=0, J'=0-13)$, $\text{H}(\text{fast}) + \text{D}_2 \rightarrow \text{HD}(v'=1, J'=1-10)$, $\text{H}(\text{fast}) + \text{D}_2 \rightarrow \text{HD}(v'=2, J'=1-5)$, and $\text{H}(\text{slow}) + \text{D}_2 \rightarrow \text{HD}(v'=0, J'=0-5)$. Because the results of a complete quantum-mechanical calculation for this reaction have not been published, we must assume a reasonable form for the state-to-state differential cross sections to simulate the D-atom velocity distribution. First, we assume that every state-to-state reaction occurs with a hard-sphere differential cross section:

$$\frac{1}{\sigma_{vJ \rightarrow v'J'}} \frac{d\sigma_{vJ \rightarrow v'J'}}{d\Omega} = \frac{1}{4\pi} \quad (14)$$

In this case, the calculated velocity distribution, convoluted with our instrument function is given as the dashed line in Figure 10. Second, we assume that every D_2 vibrational state to HD vibrational state reaction occurs with the same J' -dependent differential cross sections as those calculated by Zhang and Miller⁴⁴ for the $\text{D} + \text{H}_2(v=0, J=0) \rightarrow \text{HD}(v'=1, J') + \text{H}$ reaction at a collision energy of 1.25 eV. In this case, the expected velocity distribution is given by the solid line in Figure 10. Although the assumption of a hard-sphere cross section is clearly too crude, the agreement with the cross sections calculated by Zhang and Miller is excellent. Although these cross sections should be used to model the H-atom velocity distribution for the $\text{D} + \text{H}_2(v=0, J=0) \rightarrow \text{HD}(v'=1, J') + \text{H}$ reaction, it is perhaps surprising that they work so well for the D-atom distribution of the $\text{H} + \text{D}_2(v=0, J) \rightarrow \text{HD}(v', J') + \text{D}$ reaction. This agreement does not imply that the differential cross sections are the same, but rather that the velocity distribution of the atomic product is not overly sensitive to the reaction dynamics.

This paper has demonstrated the feasibility of using (1 + 1 + 1) 2D-REMPI-TOF to determine full three-dimensional velocity distributions of the D-atom product of the $\text{H} + \text{D}_2$ reaction. We believe that these measurements represent a first step to the determination of alignment-dependent state-to-state differential cross sections for the $\text{H} + \text{D}_2 \rightarrow \text{HD}(v', J') + \text{D}$ reaction.

Acknowledgment. R.P.T. thanks the Fulbright Commission for a Senior Research Scholarship, and M.S. thanks the Center for Materials Research, Stanford University, for a Scholarship. This work is supported by the National Science Foundation under grant NSF CHE-89-21198.

Appendix

A.1. Impulse-Extraction TOF Detection of Ions. In a TOF mass spectrometer, Loo et al.³¹ and Hwang and El-Sayed⁴⁵ have shown that a pulsed extraction field can be used to improve velocity resolution of products from a unimolecular photodissociation process. We have also achieved improved resolution with a pulsed, rather than a static field. In this section we explain differences between our technique, which we call "impulse-extraction TOF" spectrometry, and the technique used by these two groups, which we call "pulsed-extraction TOF" spectrometry. We also present an analytical expression for the TOF of an ion when the pulse is a square wave.

In both techniques, ions are created in a field-free region between extractor and repeller plates (Figure 4). A pulsed voltage is then applied to either the extractor or the repeller plate to create a uniform field. In the pulsed-extraction technique, an ion is allowed to travel for a fixed time before the field is applied

to accelerate the ion from the extraction region into a field-free TOF tube. The position of the ion when the extraction field is applied determines its energy when it enters the TOF tube. This energy difference translates into a velocity-dependent TOF profile.

The fact that ions in a pulsed-extraction technique disperse in the probe region may prove problematic in the study of a photoinitiated bimolecular reaction. The space charge induced by the pump and probe lasers may cause the ions to acquire a range of kinetic energies as they move into different regions of this nonuniform field. To minimize this effect, we use a pulsed field that is applied *immediately* after the probe lasers have created the ions. This field removes the ions from the probe region before they have a chance to spread significantly in space. To improve velocity resolution, the field is turned off before any ions leave the extraction region. Because the field is applied after all the ions are created and is turned off before any ions leave the extraction region, each ion is accelerated by the same amount, independent of its original position, time of creation, and velocity. The drift tube velocity, v_{TOF} , is therefore given by

$$v_{\text{TOF}} = v_z + v_a \quad (\text{A.1})$$

where v_a is the integration of the acceleration from the pulsed field over the time of the pulse, and v_z is the initial axial velocity of the ion. (The z axis is defined so that positive values of v_z correspond to motion toward the detector, negative values of v_z to motion away from the detector.)

To understand why our impulse-extraction technique leads to better velocity resolution than would a static extraction field, we consider two ions, A and B, of the same mass and charge created in a static field with equal speeds along the TOF axis. Ions A and B differ only in that when they are created, A is traveling toward the detector, and B is traveling away from the detector. While A travels to the detector, B's direction is reversed by the applied field. When B returns to its starting point, it has a velocity that is equal to the initial velocity of A. From this point, B follows the exact trajectory as A, but delayed by the turnaround time. Thus the flight time of A and B will differ by a constant amount, and will be independent of the length of the TOF drift tube. This situation differs from impulse-extraction, in which the difference between the velocity of A and B remains constant for the entire flight time. In this case the full length of the field-free TOF tube is used to resolve the velocities of A and B.⁴⁶

If we assume an extraction field that is created by a square-wave voltage pulse of height V_p that turns on at time $t = 0$ and turns off at time $t = t_p$, the TOF of an ion can be calculated in a straightforward manner. The TOF of an ion created with a velocity v_z at a time t_1 before the voltage pulse is turned on (i.e., at $t = -t_1$) is given by

$$t = \frac{X - v_z t_1 + \frac{1}{2} a_p t_p^2}{a_p t_p + v_z} \quad (\text{A.2})$$

or equivalently,

$$t = \frac{X - v_z t_1 + \frac{1}{2} v_a t_p}{v_a + v_z} \quad (\text{A.3})$$

Here $X = d + L$, where d is the distance from the ionization region to the exit of the extraction region, L is the distance from the extraction region to the detector (Figure 4), and a_p is the acceleration caused by the pulsed field. Here v_a , which is equal to $a_p t_p$, is given by

$$v_a = \frac{e}{mD} \int_{-\infty}^{\infty} V(t') dt' \quad (\text{A.4})$$

which for a square-wave pulse reduces to

$$v_a = eV_p t_p / mD \quad (\text{A.5})$$

Here e and m are the charge and mass of the ion, and D is the distance between the extractor and repeller plates. Note that eqs A.2–5 only apply when the ion is created before the field is turned on and does not leave the extraction region before the field is turned off. This requirement is met when

$$t_p < \left(\frac{Dm}{eV_p} \right) (-v_z + [v_z^2 + 2deV_p/mD]^{1/2}) \quad (\text{A.6})$$

Equations A.3 and A.5 tell us that the TOF of an ion depends on its charge-to-mass ratio, its initial axial velocity, the geometry of the TOF analyzer, and the values of V_p and t_p . In practice, it is never possible to apply a perfect square-wave pulse. However, this is unimportant because any arbitrarily shaped voltage pulse that starts after $t = t_0$ and stops before $t = t_p$ is equivalent to a square-wave pulse (Appendix A.3). Effective values of V_p and t_p are obtained by digitizing the voltage profile with an oscilloscope (see Appendix A.3). We can then compare the experimental TOF peak positions with those predicted by eq A.3. Because our high-voltage probe has limited bandwidth (~ 50 MHz) and accuracy ($\sim 3\%$), it is sometimes necessary to adjust the effective values of V_p and t_p by up to 5% to fit the TOF peak positions. The parameters we use to fit the H-atom and D-atom TOF profiles are given in columns 3 and 5 of Table 1.

A.2. The Instrument Function. In the previous section, we assumed zero radial velocity of the ion and a perfect TOF analyzer. For each value of v_z , therefore, the ion has a single value for its TOF with no error. In practice, broadening of v_x and v_y about their values of zero (caused by the finite bandwidths of the probe lasers), and uncertainties in V_p , X , and t_1 degrade the TOF profile. In this section we derive the relationship between the three-dimensional velocity distribution, $f(v)$, and the 2D-REMPI-TOF profile we actually observe $g_{\text{exp}}(t)$.

If the two probe lasers have infinitely narrow bandwidths, the observed TOF profile would map directly into the velocity distribution we wish to measure, but we would only probe the infinitesimally small fraction of molecules with $v_x = v_y = 0$. Instead, through judicious use of etalons, we set the bandwidth of these lasers to compromise between resolution and the number of ions we are able to produce. Because of the simple form of eq A.3, realistic predictions of experimentally determined velocity distributions can be made without resorting to Monte Carlo simulations. To determine an expected velocity distribution, $f_{\text{calc}}(v)$, that can be compared to a measured velocity distribution, three steps are involved (Figure 11). They are (1) convolution of the velocity distribution with the resolution of our 2D-REMPI probe to find the expected axial velocity distribution, $f_{xy}(v_z)$; (2) convolution of $f_{xy}(v_z)$ with the instrument function, which we label $I(t, v_z)$, to obtain the expected TOF spectrum, $g_{\text{calc}}(t)$; and (3) Jacobian transformation of $g_{\text{calc}}(t)$ to find $f_{\text{calc}}(v)$. A comparison of either $g_{\text{calc}}(t)$ to $g_{\text{exp}}(t)$ or $f_{\text{calc}}(v)$ to $f_{\text{exp}}(v)$ provides a test of the ability of $f(v)$ to describe the dynamics of a unimolecular photodissociation or a bimolecular reaction. We consider each of these steps in detail.

1. Convolution of $f(v)$ with the Resolution of the 2D-REMPI Probe. Because we can measure the line shape of our lasers and are careful not to saturate either of the two resonant transitions, our velocity resolution in the xy plane of the probe lasers is extremely well-defined. If we fit our laser line shapes to a Gaussian profile, we can write down the relationship between the full velocity distribution of the probed molecule, $f(v)$, and the axial velocity

distribution of the ions that we create, $f_{xy}(v_z)$:

$$f_{xy}(v_z) = \int_{-\infty}^{\infty} \int_{-\infty}^{\infty} f(v) \exp \left[-4 \ln 2 \left(\left(\frac{v_x - v'_x}{\Delta v_x} \right)^2 + \left(\frac{v_y - v'_y}{\Delta v_y} \right)^2 \right) \right] dv'_x dv'_y \quad (\text{A.7})$$

Here v_x is the Doppler-selected velocity in the x direction, v_y is the Doppler-selected velocity in the y direction, and Δv_x and Δv_y give the full width at half-maximum of our velocity selection as determined by the bandwidths of the probe lasers.¹² If $f(v)$ is normalized to unity, $f_{xy}(v_z)$ is normalized in such a way that

$$f_+ = \frac{n_+}{n} = \phi_+ \int_{-\infty}^{\infty} f_{xy}(v_z) dv_z \quad (\text{A.8})$$

Here, f_+ is the ratio of the density of ions produced, n_+ , to the density of probed molecules in the ionization region, n . The probability that a stationary molecule in the probed volume is selected by 2D-REMPI when the probed lasers are tuned to resonance is denoted by ϕ_+ .

2. Convolution of $f_{xy}(v_z)$ with the Instrument Function. The relationship between the velocity distribution $f_{xy}(v_z)$, the TOF profile, $g_{\text{calc}}(t)$, and the instrument function, $I(t, v_z)$ is

$$g_{\text{calc}}(t) = \int_{-\infty}^{\infty} I(t, v_z) f_{xy}(v_z) dv_z \quad (\text{A.9})$$

The resolution of our TOF profile is limited by our ability to fix the experimental parameters in eq A.3. To obtain an analytical formula for $I(t, v_z)$, we consider only the uncertainty in the TOF distance, ΔX , in the delay between the ionization laser and the rise in the voltage pulse, Δt_1 , and in the velocity imparted by the pulser, Δv_a . ΔX is determined by the finite beam waste of our cylindrically focused v_y laser, Δt_1 is determined by the 7-ns pulse width of our probe lasers and the jitter in the firing of the lasers, and Δv_a ($= e t_p \Delta V_p / mD$) is caused by the nonideal ion optics in the extraction region. Unfortunately, we have no direct way of quantifying ΔV_p . Instead, Δv_a is a free parameter of the fit. Because the profile of our pulser is extremely stable, we ignore the uncertainty in t_p . We make the additional simplifying assumption that the spread in each of these three variables is Gaussian. Under these conditions, the instrument function is given by

$$I(t, v_z) = \frac{1}{(4\pi \ln 2)^{3/2} \Delta X \Delta t_1 \Delta v_a} \times \\ \int_{-\infty}^{\infty} \int_{-\infty}^{\infty} \int_{-\infty}^{\infty} \exp \left[-4 \ln 2 \left(\left(\frac{X - X'}{\Delta X} \right)^2 + \left(\frac{t_1 - t'_1}{\Delta t_1} \right)^2 + \left(\frac{v_a - v'_a}{\Delta v_a} \right)^2 \right) \right] \delta \left(t - \frac{X' - v_z t'_1 + 1/2 v'_a t_p}{v'_a + v_z} \right) dX' dt'_1 dv'_a \quad (\text{A.10})$$

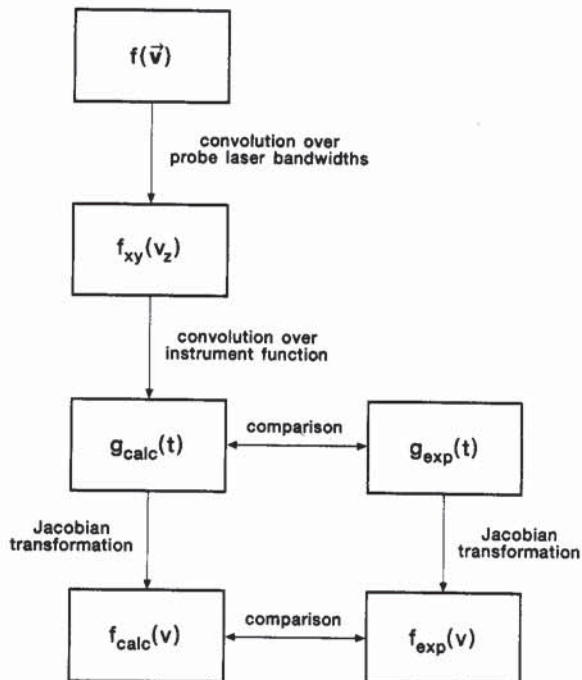
If we make the approximation that the TOF velocity, $v_z + v'_a$, is greater than zero for every value of v'_a for which the integrand does not vanish, then this three-dimensional integral reduces to

$$I(t, v_z) = \left(\frac{2(\ln 2)^{1/2}}{\pi^{1/2} (t + t_1)^2 \Delta v_z} \right) \left[(t + t_1)(v_z + v_a) + \left(\frac{\Delta v_a}{\Delta v_z} \right)^2 (t - 1/2 t_p)(v_z(t) - v_z) \right] \exp \left[-4 \ln 2 \left(\frac{v_z - v_z(t)}{\Delta v_z} \right)^2 \right] \quad (\text{A.11})$$

TABLE 1: Time-of-Flight Parameters for the Detection of H and D Atoms^a

parameter	explanation	H-atom detection		D-atom detection	
		value	uncertainty	value	uncertainty
X/cm ($L + d$)	distance from ionization region to end of TOF tube	9.17	0.01	9.17	0.01
D/cm	distance between extractor and repeller plates	3.03	—	3.03	—
V _{eff} /V	voltage pulse height	288.7 ^b	4.0	349.7 ^b	5.0
t _p ² /ns	voltage pulse width	98.20 ^b	—	109.77 ^b	—
v _a /km·s ⁻¹	velocity imparted by pulser	89.68 ^c	1.2 ^d	60.78 ^c	0.9 ^d
t ₁ /ns	probe laser-voltage pulse time delay	28.45	12.0	20.0	5.0
S/cm	distance from end of TOF tube to detector	0.76	—	0.76	—
V _s /V	voltage drop to detector	-1703	—	-1850	—

^a Distances and voltages illustrated in Figure 4. ^b Adjusted by as much as 5% from measured value to fit to data. ^c Not an independent parameter ($v_a = eV_p t_p / mD$). ^d Free parameter of fit to data.



THEORY

EXPERIMENT

Figure 11. Flow chart of the procedure for comparing a theoretical velocity distribution, $f(v)$, to experimental data.

Here $v_z(t)$ is obtained by inverting eq A.3,

$$v_z(t) = \frac{X - (t - 1/2t_p)v_a}{t + t_1} \quad (\text{A.12})$$

and

$$\Delta v_z = \left(\frac{\Delta v_a^2 (t - 1/2t_p)^2 + \Delta X^2 + \Delta t_1^2 v_z^2}{(t + t_1)^2} \right)^{1/2} \quad (\text{A.13})$$

Two adjustments must be made before the calculated TOF profile, $g_{\text{calc}}(t)$, can be compared to experimental data. First, a small correction is made for the time it takes for the ion to travel the small distance between the end of the TOF tube and the detector. Second, as mentioned earlier, we adjust our effective values of t_p and V_p by as much as 5% and treat Δv_a as a free parameter to fit the data. We find the best fit occurs when Δv_a corresponds to an uncertainty in ΔV_p of $\sim 0.01 V_p$. All other experimental variables are measured directly, and their values are given in Table 1.

3. *Jacobian Transformation of $g_{\text{calc}}(t)$ and $g_{\text{exp}}(t)$.* It is informative to compare the velocity distribution, $f_{\text{exp}}(v)$, to the predicted velocity distribution, $f_{\text{calc}}(v)$. A Jacobian transformation of both the predicted TOF profile and experimental data makes

this possible:

$$f_{\text{calc}}(v) = g_{\text{calc}}(t) \left| \frac{dt}{dv_z} \right| \quad (\text{A.14})$$

$$f_{\text{exp}}(v) = g_{\text{exp}}(t) \left| \frac{dt}{dv_z} \right| \quad (\text{A.15})$$

where t is given by eq A.3 and dt/dv_z is given by differentiation of this equation.

To illustrate this complete procedure, we consider a single-channel photodissociation of a translationally cold diatomic molecule by a linearly polarized monochromatic laser. In this limit, the photofragments have a velocity distribution, $f(v)$, given by

$$f(v) = \frac{\delta(v - v_0)}{4\pi v_0^2} (1 + \beta P_2(\hat{v} \cdot \hat{e})) \quad (\text{A.16})$$

v_0 is the velocity of the photofragment, β is the anisotropy parameter for the dissociation, and \hat{e} is the direction of the electric vector of the photolysis laser. For this discussion, we consider the photolysis of DI at 266 nm with a laser polarized perpendicular to the TOF axis ($\hat{e} = \hat{x}$). We only consider the channel leading to a D atom and ground-state I(²P_{3/2}) (i.e., the background signal in the experimental data presented in section 5.2). In this case $v_0 = 12.3 \text{ km}\cdot\text{s}^{-1}$, and $\beta = -1$. If the 2D-REMPI probe lasers are tuned to the line center of each of the two resonant transitions, the distribution of axial velocities of the ions, $f_{xy}(v_z)$, is given by eq A.7 with $v_x = v_y = 0$. The result of a numerical integration when $\Delta v_x = 8 \text{ km}\cdot\text{s}^{-1}$ and $\Delta v_y = 4 \text{ km}\cdot\text{s}^{-1}$ is given in Figure 12a. The integration given in eq A.9 yields the expected TOF profile, $g_{\text{calc}}(t)$, is shown in Figure 12b. Equation A.14 can then be used to find the expected velocity distribution (Figure 12c). Although both of the velocity distributions are symmetric about $v = 0$, the TOF distributions are asymmetric, with the late TOF peak having less height and more width, but the same integrated area as the early TOF peak because of the Jacobean transformation (eq A.14).

The experimental parameters used in the simulations presented in Figures 6, 7, 10, and 12 are given in Table 1.

3.3. Equivalence of Pulse Forms in Pulsed-Extraction TOF Spectrometry. Equations A.3 and A.5 apply equally well to an arbitrarily shaped pulse, $V(t)$, provided $V(t)$ is nonzero only in the time interval between t_0 and t_f where the ion is created before the field is applied ($t_0 > -t_1$) and remains in the extraction region while $t < t_f$. In this case, the time-dependent velocity of the ion can be found by integrating the acceleration, and the time-dependent position can be found by integrating its velocity. For $t > t_f$,

$$x(t) = (t + t_1)v_z + (t - t_f) \int_{t_0}^{t_f} \frac{eV(t')}{mD} dt' + \int_{t_0}^{t_f} \int_{t_0}^{t'} \frac{eV(t'')}{mD} dt'' dt' \quad (\text{A.17})$$

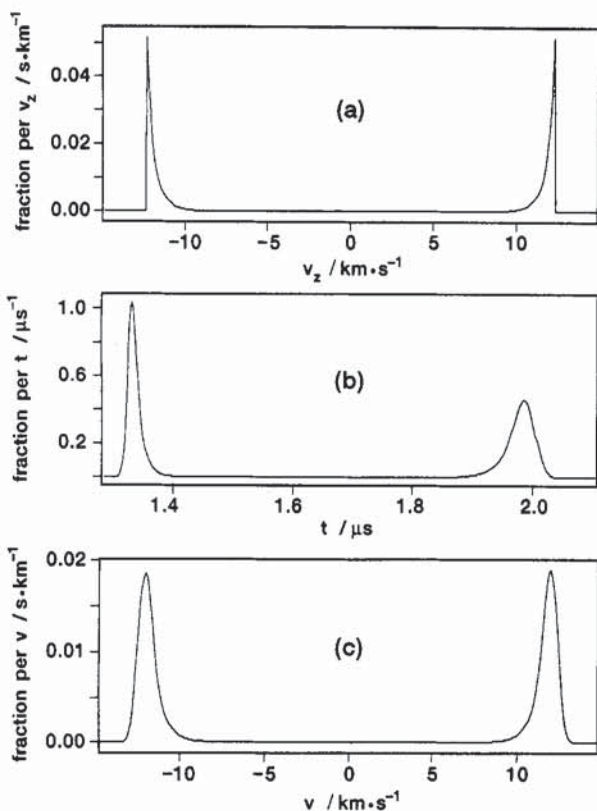


Figure 12. Calculation of the velocity distribution of D atoms from the photolysis of DI at 266 nm to produce D + I($^2P_{3/2}$): (a) axial velocity distribution of ions selected by 2D-REMPI, $f_{xy}(v_z)$; (b) TOF profile, $g_{\text{calc}}(t)$, obtained by convoluting $f_{xy}(v_z)$ with our instrument function, $I(t, v_z)$; and (c) predicted velocity distribution, $f_{\text{calc}}(v)$.

By setting $x(t)$ equal to X and the one-dimensional integral to v_a (eq A.4), we find

$$t = \frac{X - v_a t_f + v_a t_f - \int_{t_0}^{t_f} \int_{t_0}^{t'} \frac{eV(t'')}{mD} dt'' dt'}{v_a + v_z} \quad (\text{A.18})$$

We define the effective pulse duration by

$$t_p^{\text{eff}} = 2 \left(t_f - \frac{\int_{t_0}^{t_f} \int_{t_0}^{t'} V(t'') dt'' dt'}{\int_{t_0}^{t_f} V(t) dt} \right) \quad (\text{A.19})$$

and the effective pulse height by

$$V_p^{\text{eff}} = \frac{1}{t_p^{\text{eff}}} \int_{t_0}^{t_f} V(t) dt \quad (\text{A.20})$$

If we substitute t_p^{eff} and V_p^{eff} for t_p and V_p , eqs A.3 and A.5 become equivalent to eqs A.18 and A.4, respectively. Hence, we see that any pulse that satisfies the impulse-extraction conditions can be modeled exactly by a square-wave pulse. This fact has the important implication that a fast rise time does not improve the resolution. Indeed, a very rapidly changing field could be undesirable. The high-frequency components of a rapidly changing voltage increase field inhomogeneities resulting from impedance mismatches in the extraction plates and may induce a background of nonresonant ions created by rf heating.

References and Notes

- (1) Case, D. A.; McClelland, G. M.; Herschbach, D. R. *Mol. Phys.* 1978, 35, 541.
- (2) Rubahn, H.-G.; Bergmann, K. *Annu. Rev. Phys. Chem.* 1990, 41, 735.
- (3) This conclusion applies even if no internal angular momentum is transferred from the reactants to the products. In this case, $\theta_{\omega-b} = \theta_{\omega'-b'} = 0$, the ratio of the impact parameters can be determined ($b'/b = \mu\omega/\mu'\omega'$), but the absolute values of b and b' can not.
- (4) Private communications with: (a) A. Kuppermann, (b) W. H. Miller, (c) D. Neuhauser.
- (5) Buntin, S. A.; Giese, C. F.; Gentry, W. R. *J. Chem. Phys.* 1987, 87, 1443.
- (6) Buntin, S. A.; Giese, C. F.; Gentry, W. R. *Chem. Phys. Lett.* 1990, 168, 513.
- (7) Continetti, R. E. Ph.D. Thesis, University of California Berkeley, CA, 1989.
- (8) Continetti, R. E.; Balko, B. A.; Lee, Y. T. *J. Chem. Phys.* 1990, 93, 5719.
- (9) Schnieder, L.; Welge, X. *XIVth International Symposium on Molecular Beams*; Asilomar: California, 1992; p 27.
- (10) Kitsopoulos, T. N.; Buntine, M. A.; Bandwin, D. P.; Zare, R. N.; Chandler, D. W. *Science* 1993, 260, 1605.
- (11) Hall, G. E. *Twelfth Combust. Res. Conf., Tahoe City, CA*, 1990, 122.
- (12) Shafer, N. E. Ph.D. Thesis, Columbia University, New York, 1990.
- (13) Brouard, M.; Duxon, S. P.; Enriquez, P. A.; Simons, J. P. *J. Chem. Phys.* 1992, 97, 7414.
- (14) Aoiz, F. J.; Brouard, M.; Enriquez, P. A.; Sayos, R. *J. Chem. Soc., Faraday Trans.* 1993, 89, 1427.
- (15) Brouard, M.; Duxon, S. P.; Enriquez, P. A.; Simons, J. P. *J. Chem. Soc., Faraday Trans.* 1993, 89, 1435.
- (16) Shafer, N. E.; Orr-Ewing, A. J.; Simpson, W. R.; Xu, H.; Zare, R. N. *Chem. Phys. Lett.* 1993, 212, 155.
- (17) Simpson, W. R.; Orr-Ewing, A. J.; Zare, R. N. *Chem. Phys. Lett.* 1993, 212, 163.
- (18) Orr-Ewing, A. J.; Zare, R. N. In *Chemical dynamics and kinetics of small radicals*; Wagner, A., Liu, K., Eds.; World Scientific: Singapore.
- (19) Rinnen, K.-D.; Kliner, D. A. V.; Zare, R. N.; Huo, W. M. *Isr. J. Chem.* 1989, 29, 369.
- (20) Rinnen, K.-D.; Buntine, M. A.; Kliner, D. A. V.; Zare, R. N.; Huo, W. M. *J. Chem. Phys.* 1991, 95, 214.
- (21) Huo, W. M.; Rinnen, K.-D.; Zare, R. N. *J. Chem. Phys.* 1991, 95, 205.
- (22) Vrakking, N. J. J.; Braker, A. S.; Suzuki, T.; Lee, Y. T. *Rev. Sci. Instrum.* 1993, 64, 645.
- (23) Blake, R. S.; Rinnen, K.-D.; Kliner, D. A. V.; Zare, R. N. *Chem. Phys. Lett.* 1988, 153, 365.
- (24) Rinnen, K.-D.; Kliner, D. A. V.; Blake, R. S.; Zare, R. N. *Chem. Phys. Lett.* 1988, 153, 371.
- (25) Adelman, D. E.; Xu, H.; Zare, R. N. *Chem. Phys. Lett.* 1993, 203, 573.
- (26) Xie, J.; Zare, R. N. *J. Chem. Phys.* 1992, 97, 2891.
- (27) Rinnen, K.-D.; Kliner, D. A. V.; Blake, R. S.; Zare, R. N. *Rev. Sci. Instrum.* 1989, 60, 717.
- (28) Allison, A. C.; Dalgarno, A. *Atomic Data* 1970, 1, 289.
- (29) Shafer, N. E.; Bersohn, R. *J. Chem. Phys.* 1991, 94, 4817.
- (30) Spliglanin, T. A.; Chandler, D. W. *Chem. Phys. Lett.* 1987, 141, 428.
- (31) Ogorzalek Loo, R.; Hall, G. E.; Haerri, H.-P.; Houston, P. L. *J. Phys. Chem.* 1988, 92, 5.
- (32) Okada, T.; Aoi, T.; Maeda, M.; Muraoka, K. *Jpn. J. Appl. Phys., Part 1* 1988, 27, 1550.
- (33) Strauss, C. E. M.; Funk, D. J. *Opt. Lett.* 1991, 16, 1192.
- (34) Mukamel, S.; Jortner, J. *J. Chem. Phys. Lett.* 1974, 29, 169.
- (35) Mukamel, S.; Jortner, J. *J. Chem. Phys.* 1974, 61, 5348.
- (36) Clear, R. D.; Riley, S. J.; Wilson, K. R. *J. Chem. Phys.* 1975, 63, 1340.
- (37) Schmiedl, R.; Dugan, H.; Meier, W.; Welge, K. H. *Z. Phys. A* 1982, 304, 137.
- (38) Van-Veen, G. N. A.; Mohamed, K. A.; Baller, T.; de Vries, A. E. *Chem. Phys.* 1983, 80, 113.
- (39) Brewer, P.; Das, P.; Ondrey, G.; Bersohn, R. *J. Chem. Phys.* 1983, 79, 720.
- (40) Xu, Z.; Koplitz, B.; Wittig, C. *J. Phys. Chem.* 1988, 92, 5518.
- (41) Levy, I.; Shapiro, M. *J. Chem. Phys.* 1988, 89, 2900.
- (42) Xu, Z.; Koplitz, B.; Wittig, C. *J. Chem. Phys.* 1989, 90, 2692.
- (43) Blais, N. C.; Truhlar, D. G. *Chem. Phys. Lett.* 1983, 102, 120.
- (44) Zhang, J. Z. H.; Miller, W. H. *J. Chem. Phys.* 1989, 91, 1528.
- (45) Hwang, H. J.; El-Sayed, M. A. *Chem. Phys. Lett.* 1990, 170, 161.
- (46) Another feature of the impulse-extraction technique is that the time of flight of an ion depends upon $(m/e)^{1/2}$ instead of the more traditional result of $(m/e)^{1/2}$. This consequence may allow superior mass resolution under some circumstances.